Determination of REEs in Permanent Magnets and Their Production Chain Using ICP-MS

Laura Suárez-Criado[1], Cyril Rado[2], Delphine Losno[1,3] and Frank Vanhaecke[1]

[1]*Department of Chemistry, Atomic & Mass Spectrometry – A&MS research unit, Ghent University, Campus Sterre – building S12, De Pintelaan 270, 9000 Ghent, Belgium*

[2]*Univ. Grenoble Alpes, CEA LITEN, Grenoble 38000, France*

[3] *BRGM, F-45060 Orléans, France*

Supplementary information:

S.1. Schematic representation of magnet production chain

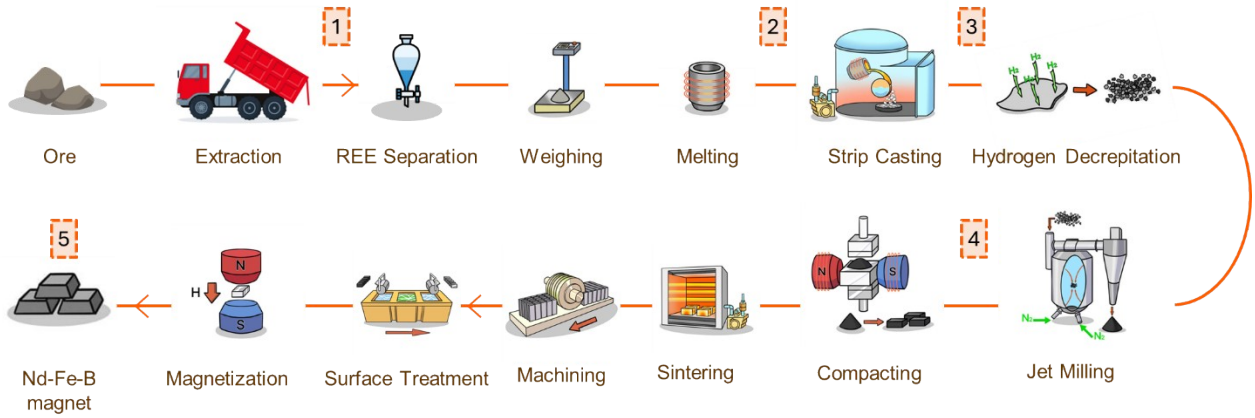

Figure S1. Scheme of the key steps of the conventional powder metallurgy process used to produce sintered Nd-Fe-B permanent magnets, the most common type on the market[39].

S.2. Additional experimental procedures

S.1.1. Evaluation of the mass of LN-Resin (100–150 µm particle size)

The optimal conditions for achieving high-resolution REE separation, as proposed by Arrigo *et al.*[21], rely on the use of 0.78 g of LN resin with 50–100 µm pore size. However, the elution process using the conditions reported takes between 9 and 12 hours. Elution times can be shortened by increasing the pore size, while also the resin mass used can have an effect on the separation efficiency.

To evaluate this, a mixture of 50 µg of the lanthanides was loaded onto LN resin with a particle size of 100–150 µm. Two different resin masses were tested: 0.78 g and 1.05 g, the former being the amount evaluated in previous studies for 50-100 µm pore size [21] and the latter representing the maximum capacity of Eichrom polypropylene columns with an 8 mm internal diameter. Element elution was carried out using the gradient optimized by Arrigo *et al.*[21] for 1.56 g of LN Resin of 100–150 µm pore size (**Table 1**). The experiment was conducted using fractions with a slightly higher molarity than the optimal value, as the HNO_3 molarity was later recalculated based on titration results (e.g., F1: 0.29 M and not 0.25 M). As a result, all elements eluted slightly earlier than under optimal conditions. However, this did not affect the selection of the optimal mass, as both masses were compared under identical conditions.

No major differences were observed in the distribution of elements across the fractions between the two resin masses used. As an example, **Figure S2** presents two graphs for Ho and Er, two elements the elution profiles of which are distributed across multiple fractions. Similar observations were made for all REEs, as their elution profiles were

similar with both resin masses. The recoveries for all elements ranged between 96.0% and 105.4% with 1.10 g of resin and between 93.6% and 108.4% with 0.78 g of resin, indicating no significant differences between the two resin masses. A resin mass of 0.78 g was selected as the optimal amount, as a smaller volume leads to a shorter elution times (ca. 7 h).

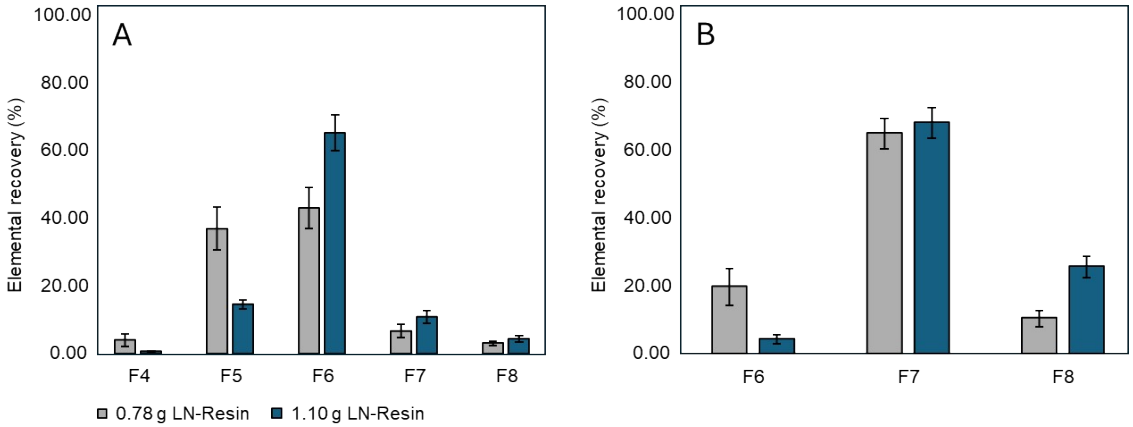

Figure S2. Distribution of elemental recovery (%) for A) Ho and B) Er across different fractions (F4-8). The gray bars represent the data with 0.78 g of LN-Resin, while the blue bars correspond to the use of 1.05 g of LN-Resin. The error bars indicate the intermediate error, expressed as the standard deviation (SD) from N = 3 replicates.

S.3. Tables

Table S1. Instrument settings for the Agilent 7900 ICP-MS.

ICP-MS Agilent 7900		
Nebulizer gas flow rate (L min^{-1})	1.05	
Integration time (s)	1	
Acquisition mode	Time-resolved analysis	
Mode	No gas mode	Gas mode
He flow rate (mL min^{-1})	-	4.60
Nuclides monitored (m/z)	^{89}Y, ^{139}La, ^{140}Ce, ^{141}Pr, ^{146}Nd, ^{147}Sm, ^{153}Eu, ^{101}Ru	^{157}Gd, ^{159}Tb, ^{163}Dy,^{165}Ho, ^{166}Er, ^{169}Tm,^{173}Yb, ^{175}Lu, ^{101}Ru

Table S2. Limits of detection achieved during the quantification of the REEs.

E	Limit of detection ($ng\ L^{-1}$)	E	Limit of detection ($ng\ L^{-1}$)
Y	0.03	**Tb**	0.01
La	0.04	**Dy**	0.03
Ce	0.04	**Ho**	0.008
Pr	0.03	**Er**	0.01
Nd	0.2	**Tm**	0.003
Sm	0.05	**Yb**	0.03
Eu	0.02	**Lu**	0.01
Gd	0.08		

Table S3. Interference table. Values in parentheses indicate the abundances of the parent nuclides at the origin of the interference. Nuclides in bold were monitored by ICP-MS.

E	Isotope	Abundance	Isobaric Interferences	Polyatomic Interferences
Y	**89**	100.00		
La	138	0.09	^{138}Ba (71.70), ^{138}Ce (0.25)	
	139	99.91		
Ce	136	0.19	^{136}Ba (7.85), ^{136}Xe (8.90)	
	138	0.25	^{138}Ba(71.70), ^{138}La (0.09)	
	140	88.48		
	142	11.08	^{140}Nd (27.13)	
Nd	142	27.13	^{140}Ce (11.08)	
	143	12.18		
	144	23.80	^{144}Sm (3.10)	
	145	8.30		
	146	17.19		
	148	5.76	^{148}Sm (11.30)	
	150	5.64	^{150}Sm (7.40)	
Pr	**141**	100		
Sm	144	3.10	^{144}Nd (23.8)	
	147	15.00		
	148	11.30	^{148}Nd (5.76)	
	149	13.80		
	150	7.40	^{150}Nd (5.64)	
	152	26.70	^{152}Gd (0.20)	
	154	22.7	^{154}Gd (2.18)	
Eu	151	47.8		
	153	52.2		^{136}CeOH^{+}
Gd	152	0.2	^{152}Sm (26.70)	^{136}CeO^{+}
	154	2.18	^{154}Sm (22.7)	^{138}CeO^{+}, ^{138}LaO^{+}
	155	14.8		^{138}LaOH^{+}, ^{138}CeOH^{+}, ^{139}LaO^{+}
	156	20.47	^{156}Dy (0.06)	^{139}LaOH^{+}, ^{140}CeO^{+}
	157	15.65		^{140}CeOH^{+}, ^{141}PrO^{+}
	158	24.84	^{158}Dy (0.10)	^{141}PrOH^{+}, ^{142}CeO^{+}, ^{142}NdO^{+}
	160	21.86	^{160}Dy (2.34)	^{143}NdOH^{+}, ^{144}NdO^{+}, ^{144}SmO^{+}

Table S3. Interference table. Values in parentheses indicate the abundances of the parent nuclides at the origin of the interference. Nuclides in bold were monitored by ICP-MS.

E	Isotope	Abundance	Isobaric Interferences	Polyatomic Interferences
Tb	**159**	100		$^{142}CeOH^+$, $^{142}NdOH^+$, $^{143}NdO^+$
Dy	156	0.06	^{156}Gd (20.47)	$^{139}LaOH^+$, $^{140}CeO^+$
	158	0.1	^{158}Gd (24.84)	$^{141}PrOH^+$,$^{142}NdO^+$, $^{142}CeO^+$
	160	2.34	^{160}Gd (21.86)	$^{144}NdO^+$, $^{144}SmO^+$
	161	18.9		$^{144}NdOH^+$, $^{144}SmOH^+$, $^{145}NdO^+$
	162	25.5	^{162}Er (0.14)	$^{145}NdOH^+$, $^{146}NdO^+$
	163	24.9		$^{146}NdOH^+$, $^{147}SmO^+$
	164	28.2	^{164}Er (1.61)	$^{147}SmOH^+$, $^{148}SmO^+$, $^{148}NdO^+$
Er	162	0.14	^{162}Dy (25.5)	$^{145}NdOH^+$, $^{146}NdO^+$
	164	1.61	^{164}Dy (28.2)	$^{147}SmOH^+$, $^{148}SmO^+$, $^{148}NdO^+$
	166	33.6		$^{149}SmOH^+$, $^{150}SmO^+$, $^{150}NdO^+$
	167	22.95		$^{150}NdOH^+$, $^{150}SmOH^+$, $^{151}EuO^+$
	168	26.8	^{168}Yb (0.13)	$^{151}EuOH^+$, ^{152}SmO, $^{152}GdO^+$
	170	14.9	^{170}Yb (3.05)	$^{153}EuOH^+$, $^{154}GdO^+$, $^{154}SmO^+$
Ho	**165**	100		$^{148}NdOH^+$, $^{148}SmOH^+$, $^{149}SmO^+$
Yb	168	0.13	^{168}Er(26.80)	$^{151}EuOH^+$, $^{152}SmO^+$, $^{152}GdO^+$
	170	3.05		$^{153}EuOH^+$, $^{154}GdO^+$, $^{154}SmO^+$
	171	14.3		$^{154}SmOH^+$, $^{154}GdOH^+$, $^{155}GdO^+$
	172	21.9		$^{155}GdOH^+$, $^{156}GdO^+$, $^{156}DyO^+$
	173	16.12		$^{156}GdOH^+$, $^{156}DyOH^+$, $^{157}GdO^+$
	174	31.8	^{174}Hf (0.16)	$^{157}GdOH^+$, $^{158}GdO^+$, $^{158}DyO^+$
	176	12.7	^{176}Hf (5.21), ^{176}Lu (2.59)	$^{159}TbOH^+$, $^{160}DyO^+$, $^{160}GdO^+$
Tm	**169**	100		$^{152}SmOH^+$, $^{152}GdOH^+$, $^{153}EuO^+$
Lu	**175**	97.41		$^{158}GdOH^+$, $^{158}DyOH^+$, $^{159}TbO^+$
	176	2.59	^{176}Hf (5.21), ^{176}Yb (12.70)	$^{159}TbOH^+$, $^{160}DyO^+$, $^{160}GdO^+$

Table S4. Recovery values for a multi-element mixture of 50 µg of REEs and Fe after using the AG® MP-1M resin.

E	Recovery (%)	E	Recovery (%)
Y	102.9 ± 2.6	**Tb**	101.5 ± 2.1
La	100.1 ± 2.0	**Dy**	102.3 ± 2.0
Ce	100.4 ± 2.4	**Ho**	101.3 ± 2.3
Pr	99.5 ± 2.7	**Er**	101.0 ± 1.8
Nd	102.0 ± 3.9	**Tm**	101.0 ± 2.2
Sm	101.6 ± 2.0	**Yb**	104.4 ± 2.6
Eu	102.0 ± 2.2	**Lu**	101.2 ± 2.2
Gd	104.0 ± 2.6	**Fe**	99.1 ± 1.6

Table S5. REE concentrations in Nd–Fe–B magnets (BRG) samples before and after chromatographic isolation. Values represent the mean ± SD for N = 6 replicates.

	Ce (%) ± SD	Nd (%) ± SD	Pr (%) ± SD
Bulk solution (before separation)	1.12 ± 0.05	21.24 ± 0.45	6.09 ± 0.12
After chromatographic isolation	1.09 ± 0.04	21.20 ± 0.74	6.07 ± 0.17

Table S6. Relative LREE abundances ($REE_i/\Sigma REE$) for Bayan Obo (BO), Mountain Pass (MP) concentrates, magnets (from BRGM, GTK and CEA), and samples from the value chain provided by CEA. Values marked with an asterisk (*) (marked in red) are expressed as mean ± standard deviation in wt% of ΣREE, whereas values without an asterisk are expressed as mean ± standard deviation in $\mu g \cdot g^{-1}$ relative to ΣREE. Uncertainties on $REE_i/\Sigma REE$ ratios were calculated by propagating the uncertainties on both REE_i and ΣREE. "< P.B." indicates values below the procedural blank.

	La ($\mu g \cdot g^{-1}$)	Ce ($\mu g \cdot g^{-1}$)	Nd ($\mu g \cdot g^{-1}$)	Pr ($\mu g \cdot g^{-1}$)	Sm ($\mu g \cdot g^{-1}$)	Eu ($\mu g \cdot g^{-1}$)	Gd ($\mu g \cdot g^{-1}$)
MP Concentrate	33.67 ± 0.17*	48.66 ± 0.5*	12.199 ± 0.057*	4.182 ± 0.044*	0.837 ± 0.026*	0.1141 ± 0.006*	0.2017 ± 0.0042*
BO Concentrate	27.11 ± 0.53*	49 ± 1.5*	16.74 ± 0.40*	5.016 ± 0.092*	1.119 ± 0.046*	0.2062 ± 0.0064*	0.4061 ± 0.0061*
Magnet 1 (BRGM)	2.118 ± 0.027*	3.69 ± 0.14*	70.62 ± 0.44*	20.37 ± 0.22*	36.9 ± 1.6	0.35 ± 0.016	0.745 ± 0.058*
Magnet 2 (BRGM)	2.201 ± 0.087*	3.70 ± 0.15*	70.2 ± 1*	20.11 ± 0.6*	33.6 ± 2	0.318 ± 0.032	1.259 ± 0.087*
Magnet 3 (BRGM)	2.114 ± 0.022*	3.67 ± 0.12*	70.7 ± 1.2*	20.38 ± 0.38*	36.4 ± 2.1	0.291 ± 0.029	0.741 ± 0.082*
Magnet 4 (GTK)	61.5 ± 1.7	39.3 ± 2.1*	46.1 ± 1.1*	11.73 ± 0.26*	16.87 ± 0.76	5.38 ± 0.79	2.25 ± 0.24*
Magnet 5 (GTK)	61.3 ± 1.9	38.8 ± 1.1*	46.5 ± 2.5*	12.02 ± 0.65*	16.1 ± 1.6	6.7 ± 1.3	2.094 ± 0.073*
Magnet 6 (GTK)	57.3 ± 2.1	39.1 ± 1.6*	46.3 ± 3.6*	11.81 ± 0.96*	16.3 ± 2.2	4.72 ± 0.97	2.182 ± 0.08*
Magnet 7 (CEA)	153 ± 27	701 ± 57	77.6 ± 3.1*	21 ± 1*	91 ± 15	< P.B.	12.8 ± 1.7
Magnet Powder (CEA)	146 ± 21	645 ± 50	78.8 ± 3.1*	21.67 ± 0.99*	112 ± 12	< P.B.	11.9 ± 1.7
Ribbon 3 (CEA)	145 ± 13	674 ± 73	78.1 ± 3.6*	22.6 ± 1.9*	42.1 ± 8.6	< P.B.	12.2 ± 1.7
Nd-Pr Alloy (CEA)	221.6 ± 5.1	332 ± 18	77.3 ± 1.9*	20 ± 2*	36.1 ± 3.7	< P.B.	7.38 ± 0.31
Ribbon 1 (Japan)	142 ± 11	286 ± 32	71.9 ± 1.2*	17.41 ± 0.68*	40 ± 10	< P.B.	35.4 ± 2.2
Ribbon 2 (Europe)	167 ± 11	385 ± 42	70.6 ± 1.6*	18.01 ± 0.84*	46 ± 14	< P.B.	14.88 ± 0.8

Values are expressed in $\mu g \cdot g^{-1}$ unless marked with * (expressed in %).

Table S7. Relative HREE abundances ($REE_i/\Sigma REE$) for Bayan Obo (BO), Mountain Pass (MP) concentrates, magnets (from BRGM, GTK and CEA), and samples from the value chain provided by the CEA. Values marked with an asterisk (*) (marked in red) are expressed as mean ± standard deviation in wt% of ΣREE, whereas values without an asterisk are expressed as mean ± standard deviation in $\mu g \cdot g^{-1}$ relative to ΣREE. Uncertainties on $REE_i/\Sigma REE$ ratios were calculated by propagating the uncertainties on both REE_i and ΣREE. "< P.B." indicates values below the procedural blank.

	Tb ($\mu g \cdot g^{-1}$)	Dy ($\mu g \cdot g^{-1}$)	Ho ($\mu g \cdot g^{-1}$)	Er ($\mu g \cdot g^{-1}$)	Tm ($\mu g \cdot g^{-1}$)	Yb ($\mu g \cdot g^{-1}$)	Lu ($\mu g \cdot g^{-1}$)	Y ($\mu g \cdot g^{-1}$)
MP Concentrate	108.1 ± 4.1	329 ± 5	34.39 ± 0.51	50 ± 5	6.34 ± 0.64	16.5 ± 1.6	1.24 ± 0.12	827 ± 79
BO Concentrate	311 ± 38	986 ± 15	99.7 ± 2.9	127 ± 13	2.61 ± 0.26	6.9 ± 0.7	0.59 ± 0.06	2158 ± 37
Magnet 1 (BRGM)	935 ± 42	1.830 ± 0.028*	0.526 ± 0.051*	8.03 ± 0.68	0.648 ± 0.019	0.262 ± 0.022	2.458 ± 0.068	76 ± 16
Magnet 2 (BRGM)	758 ± 55	2.06 ± 0.09*	0.385 ± 0.021*	8.59 ± 0.37	0.795 ± 0.026	0.281 ± 0.023	2.935 ± 0.041	84.9 ± 4.1
Magnet 3 (BRGM)	897 ± 14	1.790 ± 0.015*	0.511 ± 0.016*	8.9 ± 1.5	0.6161 ± 0.0063	0.292 ± 0.034	2.336 ± 0.055	62.8 ± 4.5
Magnet 4 (GTK)	4.24 ± 0.49	52.1 ± 1.2	0.605 ± 0.066*	3.014 ± 0.096	0.605 ± 0.096	1.32 ± 0.11	2.27 ± 0.33	67.3 ± 9.9
Magnet 5 (GTK)	4.73 ± 0.55	45.3 ± 4.6	0.613 ± 0.036*	2.99 ± 0.31	0.645 ± 0.066	1.52 ± 0.91	2.9 ± 0.3	62 ± 2
Magnet 6 (GTK)	4.48 ± 0.22	49.3 ± 3.8	0.634 ± 0.016*	2.68 ± 0.46	0.717 ± 0.076	1.19 ± 0.13	2.08 ± 0.22	61.9 ± 2.9
Magnet 7 (CEA)	26.8 ± 5.6	1.29 ± 0.088*	1.4 ± 0.1	0.191 ± 0.065	0.0218 ± 0.0073	0.099 ± 0.023	0.25 ± 0.13	4.78 ± 0.21
Magnet Powder (CEA)	25.7± 4.8	195 ± 22	0.214 ± 0.045	0.149 ± 0.035	0.012 ± 0.002	< P.B.	0.0172 ± 0.0024	4.04 ± 0.13
Ribbon 3 (CEA)	27.9 ± 7.2	954 ± 81	0.38 ± 0.12	0.152 ± 0.039	0.0164 ± 0.0089	< P.B.	0.039 ± 0.031	4.05 ± 0.20
Nd-Pr Alloy (CEA)	14.10 ± 0.31	112.1 ± 2.4	0.0742 ± 0.0018	0.101 ± 0.011	0.0089 ± 0.0013	0.0311 ± 0.0032	0.0228 ± 0.0023	4.7 ± 0.5
Ribbon 1 (Japan)	31.2 ± 5.6	10.64 ± 0.96 *	23.6± 3.5	3.12 ± 0.66	0.927 ± 0.086	1.47 ± 0.17	17.4± 1.9	7.02 ± 0.65
Ribbon 2 (Europe)	541 ± 55	11.3 ± 0.4*	35.3 ± 1.7	1.63 ± 0.27	0.379 ± 0.007	0.256 ± 0.011	6.053 ± 0.098	5.48 ± 0.15

Values are expressed in $\mu g \cdot g^{-1}$ unless marked with * (expressed in %).

Table S8. Comparison of Nd+Pr and ΣREE (wt%) for selected CEA value-chain samples: this study (ICP-MS) vs CEA/supplier data (ICP-OES/supplier). Values are reported as mean ± standard deviation where available. Ratios correspond to (this study)/(CEA or supplier).

	Nd+Pr (%)			ΣREE (%)		
	This study	**CEA/supplier**	**Ratio**	**This study**	**CEA/supplier**	**Ratio**
Nd-Pr Alloy (CEA)	93.8 ± 2.0	99.6	0.94	93.9 ± 2.0	99.7	0.94
Ribbon 3 (CEA)	37.3 ± 1.1	33.7	1.11	37.3 ± 1.1	33.7	1.11
Ribbon 1 (Japan)	29.3 ± 0.3	27.2	1.08	32.9 ± 0.5	30.7	1.07
Ribbon 2 (Europe)	32.8 ± 0.6	28.0	1.17	37 ± 0.6	31.9	1.16

Table S9. Element-by-element comparison between this study and CEA/supplier data for selected CEA value-chain and ribbon samples. Nd and Pr are reported as $REE_i/\Sigma REE$ (wt% of ΣREE), whereas Dy, La, Ce, Sm and Tb are reported as $REE_i/\Sigma REE$ in $\mu g \cdot g^{-1}$ relative to ΣREE. Values are mean ± standard deviation where available.

	Nd (%)		Pr (%)		Dy ($\mu g \cdot g^{-1}$)		La ($\mu g \cdot g^{-1}$)		Ce ($\mu g \cdot g^{-1}$)		Sm ($\mu g \cdot g^{-1}$)		Tb ($\mu g \cdot g^{-1}$)	
	This study	**CEA /supplier**	**This study**	**CEA /supplier**	**This study**	**CEA /supplier**	**This study**	**CEA /supplier**	**This study**	**CEA /supplier**	**This study**	**CEA /supplier**	**This study**	**CEA /supplier**
Nd-Pr Alloy (CEA)	77.3 ±1.9	78.6	22.6 ± 1.9	21.33			221.6 ± 5.1	220.7	332 ± 18	351	36.1 ± 3.7	200		
Ribbon 3 (CEA)	78.1 ± 3.6	77.9	21.7 ± 1.0	22.07	954 ± 80	1156								
Ribbon 1 (Japan)	71.9 ±1.3	70.7	17.4 ± 0.68	17.8	10.6 ± 1.0	11.5	142 ± 11	163	286 ± 32	260				
Ribbon 2 (Europe)					11.3 ± 0.4	12.2							541 ± 55	1876